lular carcinoma, ACE inhibitor treatment also reduced tumor development and angiogenesis.[31] In the current model of laser-induced CNV, ACE inhibition with imidapril was found to be antiangiogenic (Fig. 2), consistent with previous reports[28-30,32] showing the antiangiogenic effect of ACE inhibitors on human and rodent ischemic retinopathies. In these ocular disorders treated with ACE inhibitors, the RAS deactivation is likely to overwhelm the KKS activation, leading to antiangiogenic action in the treatment. Indeed, significant suppression of neovascularization in the choroid and the retina via inhibition of the RAS was already confirmed in our recent data from the use of AT1-R blockers.[22,33]

Of note, the ACE inhibitor-induced suppressive effect on CNV was not dose dependent (Fig. 2). This finding led us to hypothesize the possible role of bradykinin accumulated by ACE inhibition in CNV. B2-R blockade with icatibant, together with the high-dose ACE inhibition, resulted in an additively suppressive effect on CNV (Fig. 3). The data are the first to show the KKS as a positive regulator of CNV. Indeed, the major KKS component including kininogen, kallikrein, kininase II (ACE), and B2-R was shown to be present in the choroid and the retina.[34,35] Although ACE inhibition in our present data was antiangiogenic in total, the ACE inhibitor-induced activation of the KKS was suggested to play a proangiogenic role, at least in part, in diluting the suppressive effect on CNV mediated by the RAS deactivation.

Accordingly, our next focus was to examine whether the KKS contributes to CNV without ACE inhibition. The KKS has been reported to function as a positive regulator of angiogenesis.[14-17] In the murine model of hindlimb ischemia, intramuscular delivery of adenovirus containing the human kallikrein gene enhanced the ischemia-induced neovascularization.[15] In the rodent models of sarcoma and carcinoma, pharmacologic blockade of B2-R[17] and genetic depletion of kininogen or B2-R[14] reduced tumor angiogenesis and growth. Surprisingly, our present data demonstrated that B2-R blockade did not affect the development of CNV (Fig. 4). This is compatible with the data showing that the low-dose ACE inhibition failed to induce B2-R-mediated bioactivity (Fig. 3), suggesting a partial role of the KKS in the pathogenesis of CNV. The KKS activation in the development of CNV is probably minimal but is inducible when kininase II bioactivity is potently inhibited by the excessive dose of ACE inhibitors.

The molecular analyses showed that the ACE inhibitor treatment reduced the expression of CNV-related molecules including VEGF, ICAM-1, and MCP-1, whereas the B2-R blocker-induced additive decrease was observed only in VEGF expression (Fig. 5). Recent in vivo and in vitro data using pharmacologic inhibition[17] and genetic ablation[14] of B2-R have suggested that bradykinin induces VEGF via B2-R. Reasonably, B2-R-mediated VEGF expression (Fig. 5) was one of the molecular mechanisms by which the ACE inhibitor-induced activation of the KKS blunted its suppressive effect of CNV (Fig. 3). In contrast, ACE inhibitors have been shown to suppress AT1-R-mediated VEGF expression via reducing angiotensin II production.[36-38] Consistently, the present data on the ACE inhibitor-induced suppression of VEGF (Fig. 5) are supported by our recent report,[22] showing AT1-R-mediated VEGF expression in the current CNV model.

The present data showing that the ACE inhibitor imidapril was antiangiogenic in the treatment of CNV (Fig. 2) suggest that the pathogenesis of CNV is closely associated with the RAS, but minimally with the KKS. In the eye, the KKS was activated only when ACE was potently inhibited with an excessive dose. Recent clinical trials have indicated the advantages of ACE inhibitors for the treatment of hypertension and cardiovascular diseases,[39,40] also known as risk factors predisposing to AMD.[41] Reasonably, ACE inhibition, which not only reduces neovascularization in the eye but also improves the systemic background, is likely to be a novel therapeutic strategy as a preventive, early, and additive treatment for AMD. A large-scale, prospective and randomized clinical trial is awaited to validate the suppressive effect of ACE inhibition on CNV.

References

1. Klein R, Wang Q, Klein BE, Moss SE, Meuer SM. The relationship of age-related maculopathy, cataract, and glaucoma to visual acuity. *Invest Ophthalmol Vis Sci.* 1995;36:182–191.
2. Grossniklaus HE, Ling JX, Wallace TM, et al. Macrophage and retinal pigment epithelium expression of angiogenic cytokines in choroidal neovascularization. *Mol Vis.* 2002;8:119–126.
3. Sakurai E, Anand A, Ambati BK, van Rooijen N, Ambati J. Macrophage depletion inhibits experimental choroidal neovascularization. *Invest Ophthalmol Vis Sci.* 2003;44:3578–3585.
4. Tsutsumi C, Sonoda K, Egashira K, et al. The critical role of ocular-infiltrating macrophages in the development of choroidal neovascularization. *J Leukoc Biol.* 2003;74:25–32.
5. Ishibashi T, Hata Y, Yoshikawa H, Nakagawa K, Sueishi K, Inomata H. Expression of vascular endothelial growth factor in experimental choroidal neovascularization. *Graefes Arch Clin Exp Ophthalmol.* 1997;235:159–167.
6. Oh H, Takagi H, Takagi C, et al. The potential angiogenic role of macrophages in the formation of choroidal neovascular membranes. *Invest Ophthalmol Vis Sci.* 1999;40:1891–1898.
7. Krzystolik MG, Afshari MA, Adamis AP, et al. Prevention of experimental choroidal neovascularization with intravitreal anti-vascular endothelial growth factor antibody fragment. *Arch Ophthalmol.* 2002;120:338–346.
8. Gragoudas ES, Adamis AP, Cunningham ET Jr, Feinsod M, Guyer DR. VEGF Inhibition Study in Ocular Neovascularization Clinical Trial Group: pegaptanib for neovascular age-related macular degeneration. *N Engl J Med.* 2004;351:2805–2816.
9. Rosenfeld PJ, Brown DM, Heier JS, et al. Ranibizumab for neovascular age-related macular degeneration. *N Engl J Med.* 2006;355:1419–1431.
10. Yeh DC, Bula DV, Miller JW, Gragoudas ES, Arroyo JG. Expression of leukocyte adhesion molecules in human subfoveal choroidal neovascular membranes treated with and without photodynamic therapy. *Invest Ophthalmol Vis Sci.* 2004;45:2368–2673.
11. Sakurai E, Taguchi H, Anand A, et al. Targeted disruption of the CD18 or ICAM-1 gene inhibits choroidal neovascularization. *Invest Ophthalmol Vis Sci.* 2003;44:2743–2749.
12. Moreau ME, Garbacki N, Molinaro G, Brown NJ, Marceau F, Adam A. The kallikrein-kinin system: current and future pharmacological targets. *J Pharmacol Sci.* 2005;99:6–38.
13. Miura S, Matsuo Y, Saku K. Transactivation of KDR/Flk-1 by the B2 receptor induces tube formation in human coronary endothelial cells. *Hypertension.* 2003;41:1118–1123.
14. Ikeda Y, Hayashi I, Kamoshita E, et al. Host stromal bradykinin B2 receptor signaling facilitates tumor-associated angiogenesis and tumor growth. *Cancer Res.* 2001;61:5178–5185.
15. Emanueli C, Minasi A, Zacheo A, et al. Local delivery of human tissue kallikrein gene accelerates spontaneous angiogenesis in mouse model of hindlimb ischemia. *Circulation.* 2001;103:125–132.
16. Knox AJ, Corbett L, Stocks J, Holland E, Zhu YM, Pang L. Human airway smooth muscle cells secrete vascular endothelial growth factor: up-regulation by bradykinin via a protein kinase C and prostanoid-dependent mechanism. *FASEB J.* 2001;15:2180–2188.
17. Ishihara K, Kamata M, Hayashi I, Yamashina S, Majima M. Roles of bradykinin in vascular permeability and angiogenesis in solid tumor. *Int Immunopharmacol.* 2002;2:499–509.
18. de Gasparo M, Catt KJ, Inagami T, Wright JW, Unger T. International union of pharmacology. XXIII. The angiotensin II receptors. *Pharmacol Rev.* 2000;52:415–472.
19. Egami K, Murohara T, Shimada T, et al. Role of host angiotensin II type 1 receptor in tumor angiogenesis and growth. *J Clin Invest.* 2003;112:67–75.

20. Candido R, Allen TJ, Lassila M, et al. Irbesartan but not amlodipine suppresses diabetes-associated atherosclerosis. *Circulation*. 2004; 109:1536–1542.
21. Toko H, Zou Y, Minamino T, et al. Angiotensin II type 1a receptor is involved in cell infiltration, cytokine production, and neovascularization in infarcted myocardium. *Arterioscler Thromb Vasc Biol*. 2004;24:664–670.
22. Nagai N, Oike Y, Izumi-Nagai K, et al. Angiotensin II Type 1 receptor-mediated inflammation is required for choroidal neovascularization. *Arterioscler Thromb Vasc Biol*. 2006;26:2252–2259.
23. Silvestre JS, Bergaya S, Tamarat R, Duriez M, Boulanger CM, Levy BI. Proangiogenic effect of angiotensin-converting enzyme inhibition is mediated by the bradykinin B(2) receptor pathway. *Circ Res*. 2001;89:678–683.
24. Gohlke P, Kuwer I, Schnell A, Amann K, Mall G, Unger T. Blockade of bradykinin B2 receptors prevents the increase in capillary density induced by chronic angiotensin-converting enzyme inhibitor treatment in stroke-prone spontaneously hypertensive rats. *Hypertension*. 1997;29:478–482.
25. Ebrahimian TG, Tamarat R, Clergue M, Duriez M, Levy BI, Silvestre JS. Dual effect of angiotensin-converting enzyme inhibition on angiogenesis in type 1 diabetic mice. *Arterioscler Thromb Vasc Biol*. 2005;25:65–70.
26. Fabre JE, Rivard A, Magner M, Silver M, Isner JM. Tissue inhibition of angiotensin-converting enzyme activity stimulates angiogenesis in vivo. *Circulation*. 1999;99:3043–3049.
27. Takeshita S, Tomiyama H, Yokoyama N, et al. Angiotensin-converting enzyme inhibition improves defective angiogenesis in the ischemic limb of spontaneously hypertensive rats. *Cardiovasc Res*. 2001;52:314–320.
28. Moravski CJ, Kelly DJ, Cooper ME, et al. Retinal neovascularization is prevented by blockade of the renin-angiotensin system. *Hypertension*. 2000;36:1099–1104.
29. Lonchampt M, Pennel L, Duhault J. Hyperoxia/normoxia-driven retinal angiogenesis in mice: a role for angiotensin II. *Invest Ophthalmol Vis Sci*. 2001;42:429–432.
30. Tadesse M, Yan Y, Yossuck P, Higgins RD. Captopril improves retinal neovascularization via endothelin-1. *Invest Ophthalmol Vis Sci*. 2001;42:1867–1872.
31. Yoshiji H, Kuriyama S, Kawata M, et al. The angiotensin-I-converting enzyme inhibitor perindopril suppresses tumor growth and angiogenesis: possible role of the vascular endothelial growth factor. *Clin Cancer Res*. 2001;7:1073–1078.
32. Chaturvedi N, Sjolie AK, Stephenson JM, et al. Effect of lisinopril on progression of retinopathy in normotensive people with type 1 diabetes. The EUCLID Study Group. EURODIAB Controlled Trial of Lisinopril in Insulin-Dependent Diabetes Mellitus. *Lancet*. 1998; 351:28–31.
33. Nagai N, Noda K, Urano T, et al. Selective suppression of pathological, but not physiological, retinal neovascularization by blocking angiotensin II type 1 receptor. *Invest Ophthalmol Vis Sci*. 2005;46:1078–1084.
34. Igic R. Kallikrein and kininases in ocular tissues. *Exp Eye Res*. 1985;41:117–120.
35. Ma JX, Song Q, Hatcher HC, Crouch RK, Chao L, Chao J. Expression and cellular localization of the kallikrein-kinin system in human ocular tissues. *Exp Eye Res*. 1996;63:19–26.
36. Suzuki Y, Ruiz-Ortega M, Lorenzo O, Ruperez M, Esteban V, Egido J. Inflammation and angiotensin II. *Int J Biochem Cell Biol*. 2003; 35:881–900.
37. Williams B, Baker AQ, Gallacher B, Lodwick D. Angiotensin II increases vascular permeability factor gene expression by human vascular smooth muscle cells. *Hypertension*. 1995;25:913–917.
38. Fujita M, Hayashi I, Yamashina S, Fukamizu A, Itoman M, Majima M. Angiotensin type 1a receptor signaling-dependent induction of vascular endothelial growth factor in stroma is relevant to tumor-associated angiogenesis and tumor growth. *Carcinogenesis*. 2005; 26:271–279.
39. Dagenais GR, Pogue J, Fox K, Simoons ML, Yusuf S. Angiotensin-converting-enzyme inhibitors in stable vascular disease without left ventricular systolic dysfunction or heart failure: a combined analysis of three trials. *Lancet*. 2006;368:555–556.
40. The Heart Outcomes Prevention Evaluation Study Investigators. Effects of an angiotensin-converting-enzyme inhibitor, ramipril, on cardiovascular events in high-risk patients. *N Engl J Med*. 2000; 342:145–153.
41. van Leeuwen R, Ikram MK, Vingerling JR, Witteman JC, Hofman A, de Jong PT. Blood pressure, atherosclerosis, and the incidence of age-related maculopathy: the Rotterdam Study. *Invest Ophthalmol Vis Sci*. 2003;44:3771–3777.

Clinical and Experimental Ophthalmology 2007; 35: 847–854
doi: 10.1111/j.1442-9071.2007.01607.x

Original Article

Early electroretinographic features of streptozotocin-induced diabetic retinopathy

Kei Shinoda MD PhD,[1,2] Robert Rejdak MD PhD,[1,3,6] Frank Schuettauf MD,[1] Georgios Blatsios MD,[1] Michael Völker MD,[1] Naoyuki Tanimoto MD PhD,[4] Tatar Olcay MD,[1] Florian Gekeler MD,[1] Cristina Lehaci MD,[1] Rita Naskar PhD,[5] Zbigniew Zagorski MD PhD[3] and Eberhart Zrenner MD[1]

[1]University Eye Hospital, Tübingen, Germany, [2]Department of Ophthalmology, Oita University Faculty of Medicine, Oita, Japan, [3]Tadeusz Krwawicz Chair of Ophthalmology, Medical University of Lublin, Poland [4]Division of Ophthalmology and Visual Science, Graduate School of Medical and Dental Sciences, Niigata University, Niigata, Japan, [5]University Eye Hospital Munster Munster, Germany, and [6]Medical Research Centre, Polish Academy of Sciences, Warsaw, Poland

ABSTRACT

Background: This study set out to document the early electrophysiological and immunohistochemical changes that occur in the retina of experimentally induced diabetic rats.

Methods: Diabetes was induced in rats by intraperitoneal injection of 60 mg/kg of streptozotocin (STZ). Electroretinogram readings were taken monthly under either short-duration or long-duration stimuli for up to 3 months after STZ. Oscillatory potentials (OP) and the amplitudes and implicit times of a- and b-waves were analysed, and b-wave amplitudes were analysed using a Naka–Rushton fit. Scotopic a-waves were analysed with photoreceptor models, and *Rmp3* (the maximum a-wave amplitude) and S (sensitivity) were calculated. Three months after STZ injection, immunohistochemistry for glial fibrillary acidic protein was performed on the retinas of the STZ-treated rats and age-matched controls.

Results: The implicit OP times were significantly longer in the diabetic rats as compared with the controls, and this difference was noted as early as 1 month following STZ treatment. Other electrophysiological parameters, such as OP amplitudes, a- and b-wave amplitude as well as the implicit times, did not differ from controls at this stage. The sacrificed STZ-treated rats also demonstrated marked enhancement of glial fibrillary acidic protein immunoreactivity, suggesting that at least in experimentally induced diabetic retinopathy there is increased Müller cell reactivity.

Conclusion: The results of this study indicated that functional alterations in the retina develop rapidly after the onset of diabetes. Analysis of each electroretinogram component may be useful in further investigating the development mechanisms of diabetic retinopathy.

Key words: diabetic retinopathy, electroretinogram, rat, retina, streptozotocin

INTRODUCTION

Diabetic retinopathy (DR) is one of the major sight threatening diseases in adulthood,[1] and detection and monitoring the clinical signs are of the utmost importance. Some electrophysiological parameters have been shown to correlate well with advancing retinopathy and include changes to the oscillatory potentials (OP) amplitudes, as well as a- and b-wave scotopic threshold responses. Similarly, photoreceptor and post-photoreceptor abnormalities can be documented with delays in b-wave implicit times,[2–7] and alterations in the ratio between the saturation constant (logk) of the voltage and intensity function (Vlogl).[8–10] Recently early signs of neuro-retinal injury have been documented in the retinal glial cells of STZ induced diabetic rats,[11–14] These observations have included those glial elements involved with the endothelial cells and as such have implications for the blood-retinal barrier (BRB).[15,16] From an electrophysiological perspective there is known about the early changes that occur in streptozotocin (STZ)-diabetic rats prompting us to investigate those parameters which have proven useful in other models.[17–19] In addition, we sought to correlate the electrophysiological findings with histological changes using immunohistochemical staining.

■ *Correspondence.* Dr Kei Shinoda, University Eye Hospital, Calwerstr.7/1, 72076, Tuebingen, Germany. Email: shinodak@med.oita-u.ac.jp

Received 27 May 2007; accepted 27 August 2007.

METHODS

Animals

Ten of 20 male Brown Norway rats were injected intraperitoneally with STZ (60 mg/kg body weight) dissolved in 0.1% citrate buffer (pH 4.6). The remaining 10 rats, matched with the first 10 animals in age (15–16 weeks after birth), were left untreated as controls. Seven days after the injection, the onset of diabetes was confirmed by checking hyperglycaemia in excess of 250 mg/dL, polyuria, polydipsia and cessation of growth. Serum glucose concentrations were measured using an Accu-check sensor (Roche, Mannheim, Germany) after the animals had fasted overnight. The animals were housed during the study under a controlled photoperiod cycle (12 h of light, 12 h of darkness) at a constant temperature (22–25°C) and given water and food *ad libitum* in cages. The experiments and housing of the animals were in accordance with the German Law on the Protection of Animals and the ARVO statement for the Use of Animals in Ophthalmic and Vision Research.

Electroretinograms

The animals were kept in a dark room for at least 12 h and prepared under dim red illumination. They were anaesthetized with 6 mL per kg body weight of 7% chloridehydrate and placed on a specially designed stereotaxic device provided with a heated pad and electrodes (*High-Throughput Mouse-ERG*, STZ for Biomedical Optics and Functiontesting, Tuebingen, Germany[20]). The pupils were dilated with one drop of a mixture of 1.7% tropicamide and 3.3% of phenylephrine. The ground electrode was a subcutaneous needle in the tail; the reference electrode was subcutaneously placed between the eyes; active electrodes were gold wires placed on the cornea with a drop of methylhydroxypropylcellulose (methocel). Recordings were performed with an ESPION Console (Diagnosys LLC, Littleton, MA, USA). Responses were differentially amplified and filtered by a digital bandpass filter from 0.313 to 1000 Hz to yield a- and b-waves. OP of 75–300 Hz were simultaneously recorded on a different channel with a band-pass filter.

The 11 steps stimulus intensities were used according to the International Society for Clinical Electrophysiology of Vision (ISCEV) standard before and 1, 2 and 3 months after STZ treatment. Namely, 4-ms white light pulses were presented at a frequency of 0.48 Hz at 0.005, 0.02, 0.05, 0.2, 0.5, 1.0, 2.0, 5.0, 20.0, 50.0 and 200.0 cd·s/m^2. The rather high frequency was chosen to allow rapid data acquisition and minimize the overall electroretinogram (ERG) recording time. The interval between consecutive steps was approximately 1 min. For a-wave fitting analysis, 4-ms white flash of 2.7 log cd·s/m^2 was presented in the dark. This range extends above the retinal illuminance necessary to elicit a maximum a-wave before b-wave intrusion, respectively. Responses to two flashes were averaged by computer. The light pulses were delivered with a commercial Ganzfeld stimulator (ESPION ColorBurst Handheld Ganzfeld LED-stimulator, Diagnosys LLC). Responses were stored for offline analysis after an average of 15–20 individual measurements.

Electroretinogram analysis consisted of amplitude and implicit time measurements. The implicit times of the a- and b-waves and the OP were measured from stimulus onset to the peak of each wave. The amplitudes of the a-waves were measured from baseline to the troughs of the a-waves, and the amplitudes of the b-wave were determined from the troughs of the a-waves to the peaks of the b-waves. The amplitudes of the OP were measured from each preceding negative trough to the peak.

The Naka–Rushton fits for the b-wave amplitudes[21,24] were iteratively performed by a Borland Delphi-program to determine the values of n and k for each mouse until the square fit over all luminance levels reached a minimum. In the following, V_{max} is the maximum of the b-wave amplitude, k is the intensity at which the b-wave amplitude reached half-saturation, and n is a dimensionless constant related to the slope of the intensity response function.

Scotopic a-waves were analysed by fitting them to a model proposed by Hood and Birch.[25,26] Responses to short duration stimulus conditions were fitted to the equation by estimating one set of parameters: *S*, td and *Rmp3*. The fits were done on the basis of a single response only. In this study, log *S* and log | *Rmp3* | of the diabetic rats were compared with those of the control rats by fixing the values of td to the mean of the control values (4 ms).

The Student's *t*-test was used to analyse the parameters of the Naka–Rushton fit for b-waves, the parameters of a-wave fits, the amplitudes and implicit times of a- and b-waves and the OP. Differences were considered significant at $P < 0.05$.

Immunohistochemistry

Three months after the induction with STZ the rats were sacrificed and the retinae were examined and compared with age-matched controls. Paraffin sections (5 μm thick) of enucleated eyes were deparaffinated twice, each time for 10 min, in fresh xylene. The slides were transferred twice for at least 2 min each time into fresh 100% ethanol and then into 90%, 80% and 70% ethanol for 2 min in each case. The slides were then rinsed in distilled water, placed in a plastic coplin jar filled with 10 mmol/l citrate buffer, pH 6.0 for antigen retrieval using a microwave. This was followed by rinsing in phosphate-buffered saline (PBS). The sections were blocked with 10% fetal calf serum (FCS) for 30 min. Anti-rabbit glial fibrillary acidic protein (GFAP, 1:80 dilution, Sigma Chemicals, Perth, Australia) was diluted in 10% FCS, and the sections were incubated overnight at 4°C. After the slides had been rinsed three times for 5 min each time in PBS, the sections were incubated with goat anti-rabbit Cy2 antibody (Dianova, Hamburg, Germany) (1:200 in 10% FCS) for 30 min at room temperature and washed three times for 5 min each in PBS. Finally the slides were coverslipped using Mowiol containing 4′,6′-diamidino-2-phenylindole (Hoechst, Frankfurt, Germany) and viewed with the appro-

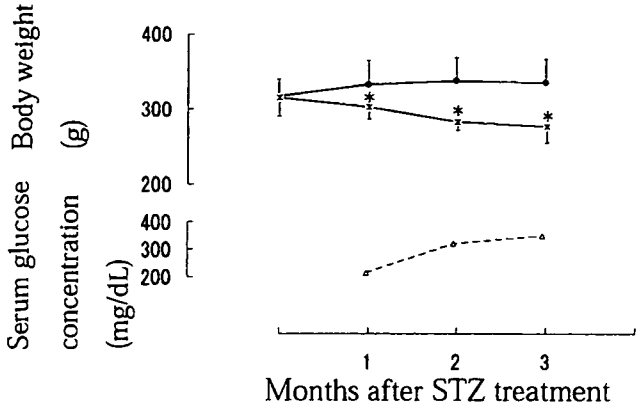

Figure 1. Mean body weight and serum glucose concentration. Upper: mean body weight in controls (closed circle, $n = 8$) and STZ-treated (star, $n = 7$) rats. Bottom: mean serum glucose concentration in STZ-treated (open triangle, $n = 7$) rats; $^*P < 0.05$. STZ, streptozotocin.

Figure 2. Dark-adapted ERG responses of a control rat (first column) and of STZ-treated rats recorded at 1, 2 and 3 months (second, third and fourth columns, respectively) after STZ injection. The stimulus intensity used to elicit each response is given in cd·s/m² to the left of each row of responses. Stimuli are shown in the lowest row. Calibration bars: vertical 100 μV and horizontal 100 ms. ERG, electroretinogram; STZ, streptozotocin.

priate filter under a microscope equipped with epifluorescence (Axiophot microscope, Carl Zeiss Inc., Thornwood, NY, USA). Control slides were treated without the primary antibodies.

Results

The electrophysiological analysis was based on the seven STZ-treated rats and the eight control rats (of an original 10 in each group) which survived the 3-month follow-up period. Three STZ-treated rats and two control animals died during the study and data relating to these animals were not included in the analysis. Those ERG data were excluded from the analysis. The STZ-treated rats were characterized by high serum glucose concentration and loss of body weight, as shown in Figure 1. No remarkable signs of cataract formation were seen in either group.

Electroretinogram

Representative dark-adapted ERG responses of a control rat and of three STZ-treated rats are shown in Figure 2. The ERG showed subnormal responses in STZ-treated rats compared with those of the controls. As illustrated in Figure 3a (intensity-response curves for a- and b-waves), the b-wave amplitudes decreased in STZ-treated rats. The intensity-response curves of the dark-adapted a-waves were less affected and were within the normal range. The implicit times of the a- and b-waves tended to increase in the STZ-treated rats, as shown in Figure 3b (plots of implicit times over the entire dynamic range [about 4–5 log units]).

The parameters of the Naka–Rushton fit are shown in Table 1. Significant differences between the control and STZ-treated rats were found only infrequently in the V_{max}. Although the k-value tended to increase in the STZ-treated rats, the increase was not statistically significant. Figure 4 shows the Naka–Rushton fit for the average b-wave amplitudes in relation to logarithmic intensity in each period. The stimulus intensities required to elicit 100 μV of a- and b-wave amplitude were determined on the basis of these figures. When the reciprocal value of the stimulus intensity for a 100 μV threshold, which can be thought of as an index of b-wave sensitivity ($S_{b\text{-}wave}$), was plotted against the time after STZ treatment, $S_{b\text{-}wave}$ appeared to drop exponentially over time. This can be well described by the equations $S_{b\text{-}wave} = 3.56 \times e^{-1.56t}$, where t is the time after STZ treatment in months (Fig. 5).

The values for S and $Rmp3$ in a model proposed by Hood and Birch[25,26] are listed in Table 1. No statistical differences in these parameters were found between the control and diabetic rats.

The representative OP are shown in Figure 6. Figure 7 and Table 1 show the amplitudes and implicit times in the control and STZ-treated rats. Delayed implicit times were observed in OP1, OP2 and OP3 of ERG responses. Implicit times showed significant changes more often and earlier than the amplitudes.

Immunohistochemistry

Glial fibrillary acidic protein immunostaining was markedly enhanced in the retinas of STZ rats compared with the age-matched control retinas. In the retinas of STZ-treated rats (3 months after STZ injection), strong GFAP immunoreactivity was observed beyond the ganglion cell layer (GCL) in Müller cell endfeet and their processes (Fig. 8b), whereas GFAP staining in the control retinas was restricted to a small band (Fig. 8a).

Discussion

It has been proposed that DR is a primary neurosensory disorder.[27] Evidence for this includes alterations in those psychophysical indices such as contrast sensitivity[28–30] and colour vision,[31,32] together with electrophysiological abnormalities[33–35] which can precede clinical signs of DR. Here the OP amplitudes were studied as well as the amplitudes and implicit times of the a- and b-waves.

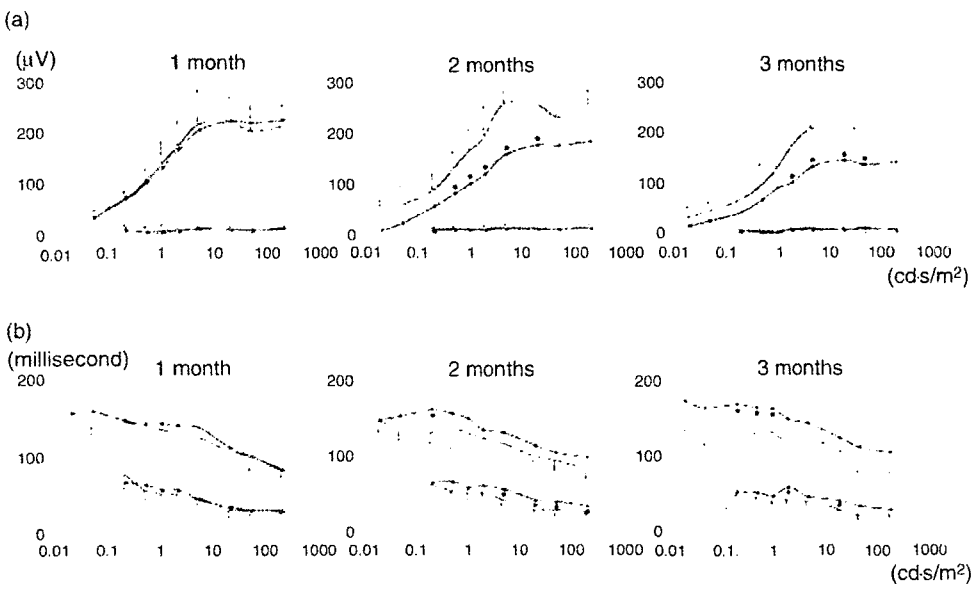

Figure 3. Intensity-response curves (a) and intensity-implicit time curves (b). The mean amplitude or mean implicit time of the a- and (triangle) b-waves (circle) in control rats ($n = 8$, open symbols) and in STZ-treated rats ($n = 7$, closed symbols) are plotted. The data were derived from ERGs performed 1, 2 and 3 months (first, second and third columns, respectively) after STZ injection. Each bar indicates standard deviation. $^{*}P < 0.05$. STZ, streptozotocin.

Table 1. The % ratio of each value in STZ rat to that in control rat

The parameters of Naka–Rushton fit on the dark-adapted b-wave			
	1 month	2 months	3 months
Vmax	95.2	73.4[a]	66.7[a]
logk	97.7	141.9	101.6
n	108.0	119.5	108.9
The parameters of a-wave fit on the dark-adapted a-wave			
	1 month	2 months	3 months
Log*Rmp3*I	105.5	95.2	96.5
Log *S*	106.2	85.9	95.1
The amplitude and implicit time of oscillatory potential			
Amplitude	1 month	2 months	3 months
Op1	90.8	39.4[a]	27.8[a]
Op2	72.2	46.0[a]	46.1[a]
Op3	84.2	59.1[a]	58.0[a]
Op4	98.8	82.9	61.2[a]
sum	82.8	57.1[a]	51.4[a]
Implicit time			
Op1	113.3[a]	116.9	120.4[a]
Op2	110.6[a]	110.9[a]	119.8[a]
Op3	110.6[a]	112.1[a]	114.0[a]
Op4	106.4	112.3[a]	117.0[a]
Sum	109.6[a]	112.7[a]	117.4[a]

$^{*}P < 0.05$ which means significant difference between STZ rat and control rat. Data are expressed as '% ratio' which was calculated as (value in STZ/value in control) × 100. STZ, streptozotocin.

The present study found early changes in several components of dark-adapted ERG responses in STZ rats. Implicit times of the OP were affected more than other parameters in the rats 1 month after STZ treatment. Li *et al.*[19] reported lower ERG response amplitudes in diabetic rats than in control rats as early as 2 weeks after the onset of diabetes. In their study, the b-wave was affected more than the a-wave. The OP appeared to be most affected in older diabetic rats (20–25 weeks). The OP are thought to originate in the inner retinal layers, although their exact cellular origin is a matter of debate.[36–38] Recent ultrastructural and immunohistochemical examinations of the STZ-treated rat retinas have revealed that some amacrine cells exhibit necrotic features 12 weeks after STZ injection.[39] This supports the thesis that OP alterations were the earliest impairment affecting electrophysiological parameters in the current study.

Recently, clear evidence of a prompt BRB breakdown (2 weeks of hyperglycaemia and increased vascular permeability) has been reported[12] after 8 days[40] or 2 weeks[10] of STZ diabetes in STZ rats, plausibly explaining the OP changes. The glial cells and blood vessels of the retina are in close apposition, and impaired vascular–glial cell interac-

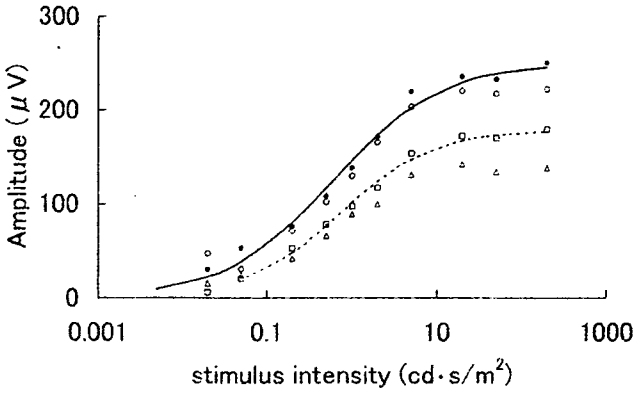

Figure 4. Naka–Rushton fit of the relation of average b-wave amplitude and logarithmic intensity in each period between control rats (closed circle, $n = 8$) and STZ-treated rats ($n = 7$). The data for STZ-treated rats were derived from ERGs performed at 1, 2 and 3 months (open circle, open square and open triangle, respectively) after STZ injection. ERG, electroretinogram; STZ, streptozotocin.

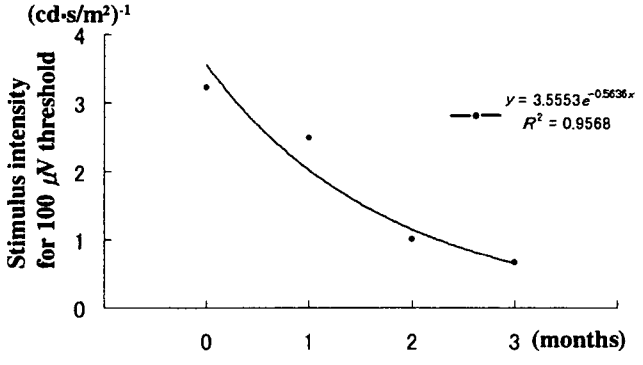

Figure 5. Stimulus intensity at the 100 μV threshold of the b-wave over time. The stimulus intensity required to elicit 100 μV of a b-wave amplitude was determined on the basis of the data in Figure 4. The reciprocal value of the stimulus intensity for 100 μV threshold, which reflects b-wave sensitivity ($S_{b\text{-}wave}$), is plotted against time after STZ treatment by month. The $S_{b\text{-}wave}$ appeared to drop exponentially over time, as expressed by $S_{b\text{-}wave} = 3.56 \times e^{-0.5630t}$ ($R^2 = 0.9568$), where t shows time after STZ treatment in months. STZ, streptozotocin.

tions at the BRB play an important role in the development of DR.[15] This agrees with clinical indications that OP amplitude changes in DR patients are directly affected by abnormal retinal vascular permeability as measured by fluorescein leakage.[33] Interestingly, Barber *et al.* demonstrated[16] an increase in permeability in the superficial arterioles and postcapillary venules 2 weeks after the onset of diabetes. This is consistent with the changes in ERG parameters in the present study. It would be interesting to investigate functional changes in relation to such changes in vascular permeability in each retinal layer.

In the current study, ERG responses recorded with short stimulus duration and short interstimulus interval, which is favourable for stimulation of the cone system, 1 month after

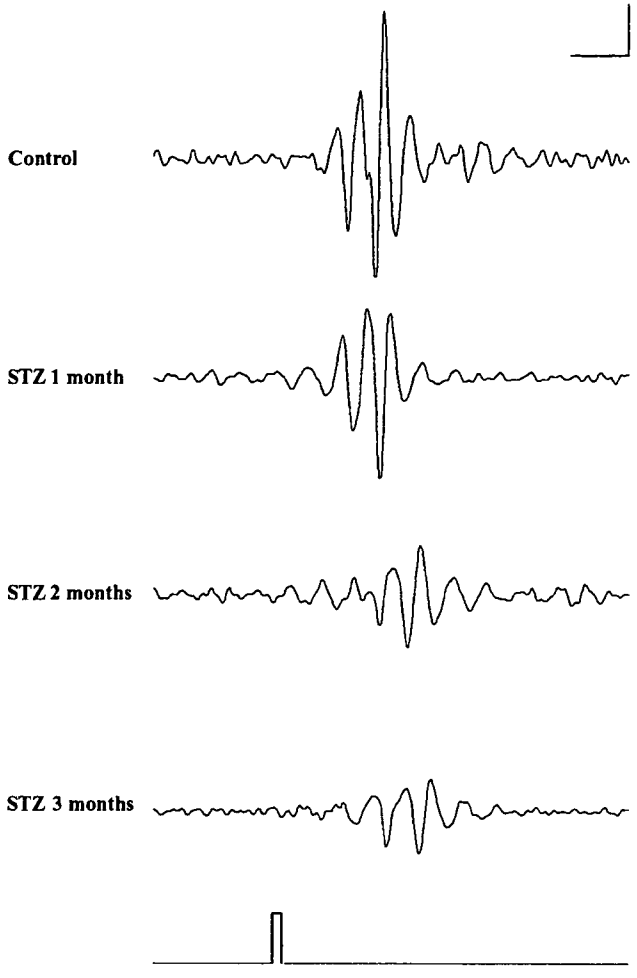

Figure 6. Oscillatory potentials recorded in the dark-adapted state in a control rat (first row) and an STZ-treated rat 1, 2 and 3 months (second row, third row and fourth row, respectively) after STZ injection. The responses were to 4-ms light pulses presented at a frequency of 0.48 Hz at 20 cd·s/m². Stimuli are shown in the lowest row. Calibration bars: vertical 10 μV, horizontal 10 ms. The results of statistical analysis of each component are listed in Table 1. STZ, streptozotocin.

STZ treatment showed delayed implicit times in OP1, OP2, and OP3. Early and late OP in humans after dark adaptation are probably generated by the cone and rod pathways, respectively.[11–13] In the current results, each OP component may reflect different photoreceptor functions. Further investigation to determine the origin of each OP, especially in rats, will be helpful to clarify this.

In accordance with a previous report,[18] the dark-adapted a-wave showed minimum alterations compared with other parameters. Phototransduction sensitivity (S) and the maximum response (Rm_{p3}) showed no significant differences between the control and STZ-treated rats. As the dark-adapted a-wave originates in the rod outer segments in rodent ERGs,[11] the photoreceptors are probably less susceptible to the pathological processes of early DR. Apoptotic features in the photoreceptor cells in the STZ rat retina have

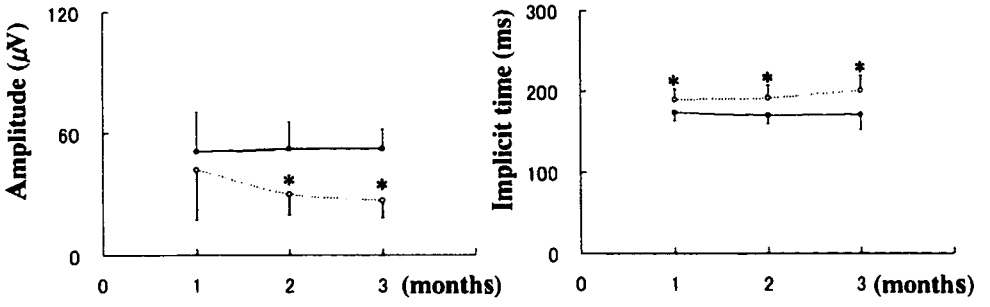

Figure 7. Sum of amplitudes and implicit times of oscillatory potentials 1–4 in control rats (open circle, $n = 8$) and STZ-treated rats (closed circle, $n = 7$). The value of each individual OP component is given in Table 1. $P < 0.05$ compared with those of the controls. STZ, streptozotocin.

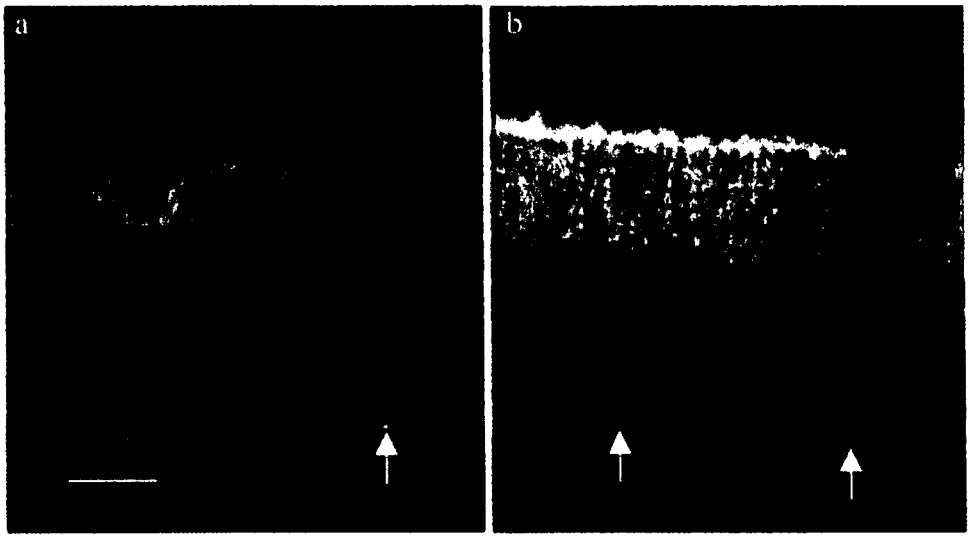

Figure 8. Glial fibrillary acidic protein (GFAP)-positive Müller cells and 4′,6′-diamidino-2-phenylindole-stained (blue) retinal neuronal nuclei in control (a) and STZ (b) retinas. The ganglion cell layer (GCL) is orientated downwards. In the STZ-treated retina, strong GFAP immunoreactivity is observed in Müller cell endfeet (white arrows) and their processes beyond the GCL (b), while GFAP staining in the control retinas is restricted to a small band (white arrows = Müller cell endfeet). An increased expression of GFAP suggests increased Müller cell reactivity induced by experimental diabetic retinopathy. Scale bar = 20 μm. Magnification: ×50. STZ, streptozotocin.

been observed 12 weeks after STZ treatment.[39] Electrophysiological evaluation after that time will be needed to clarify the functional changes in the photoreceptor cells of diabetic rat retina.

The dark-adapted b-waves are thought to be initiated by depolarization of the on-bipolar neurones in response to flash, which induces potassium efflux from the Müller cell endfeet.[45] Although morphological findings were limited in the present study, an increased expression of GFAP observed in the STZ-treated rat retina suggests that Müller cell reactivity was induced by experimental DR, which supports the likelihood of functional alteration.

The parameters of the Naka–Rushton fit showed significant changes in the STZ-treated rats only occasionally in the V_{max}. The $S_{b\text{-wave}}$, determined as the reciprocal value of the stimulus intensity required for a 100 μV threshold, decreased over time. Comparable previous studies measured dark-adapted responses with ERG in the STZ diabetic rat up to 25 weeks after STZ treatment, but statistical analysis showed no clear time-dependent changes. Li *et al.* have reported that the ratio of maximum b-wave amplitudes in diabetic rats to those of control ones fluctuated around 60% throughout the entire period of follow-up (2–25 weeks after STZ treatment). A long-term study of STZ rats will be required to determine long-term changes in the dark-adapted b-waves of STZ rats as an indicator of on-bipolar neurones and/or Müller cell functions.

ACKNOWLEDGEMENTS

The authors thank Thorsten Schwarz and D. Regelman (both from University Eye Hospital, Tuebingen) for their extremely helpful support in data analysis and Mechthild Wissing (University Eye Hospital, Münster) for carrying out the immunohistochemistry experiments and Dr Volker Vallon (Department of Pharmacology, University Tuebingen, Tuebingen) for extremely helpful advice and support in establishing STZ rat model. Kei Shinoda was supported by the Alexander von Humboldt Foundation. Robert Rejdak was supported by the European Union under a Marie Curie Individual Fellowship (QLK2-CT-2002-51562).

REFERENCES

1. Prevent Blindness America. *Vision Problems in the US: A Report on Blindness and Vision Impairment in Adults Age 40 and Older.* Schaumburg, IL: Prevent Blindness America, 1994.
2. Yonemura D, Aoki T, Tsuzuki K. Electroretinogram in diabetic retinopathy. *Arch Ophthalmol* 1962; **68**: 19–24.
3. Simonsen SE. The value of the oscillatory potential in selecting juvenile diabetics at risk of developing proliferative retinopathy. *Acta Ophthalmol* 1980; **58**: 865–78.
4. Bresnick GH, Korth K, Groo A, Palta M. Electroretinographic oscillatory potentials predict progression of diabetic retinopathy. Preliminary report. *Arch Ophthalmol* 1984; **102**: 1307–11.
5. Bresnick GH, Palta M. Predicting progression to severe proliferative diabetic retinopathy. *Arch Ophthalmol* 1987; **105**: 810–4.
6. Holopigian K, Greenstein VC, Seiple W, Hood DC, Carr RE. Evidence for photoreceptor changes in patients with diabetic retinopathy. *Invest Ophthalmol Vis Sci* 1997; **38**: 2355–65.
7. Aylward GW. The scotopic threshold response in diabetic retinopathy. *Eye* 1989; **3**: 626–37.
8. Juen S, Kieselbach GF. Electrophysiological changes in juvenile diabetics without retinopathy. *Arch Ophthalmol* 1990; **108**: 372–5.
9. Holopigian K, Seiple W, Lorenzo M, Carr R. A comparison of photopic and scotopic electroretinographic changes in early diabetic retinopathy. *Invest Ophthalmol Vis Sci* 1992; **33**: 2773–80.
10. Satoh S, Iijima H, Imai M, Abe K, Shibuya T. Photopic electroretinogram implicit time in diabetic retinopathy. *Jpn J Ophthalmol* 1994; **38**: 178–84.
11. Lieth E, Barber AJ, Xu B *et al.* Glial reactivity and impaired glutamate metabolism in short-term experimental diabetic retinopathy. Penn State Retina Research Group. *Diabetes* 1998; **47**: 815–20. Erratum in: *Diabetes* 1998; **47**: 1170.
12. Rungger-Brandle E, Dosso AA, Leuenberger PM. Glial reactivity, an early feature of diabetic retinopathy. *Invest Ophthalmol Vis Sci* 2000; **41**: 1971–80.
13. Zeng XX, Ng YK, Ling EA. Neuronal and microglial response in the retina of streptozotocin-induced diabetic rats. *Vis Neurosci* 2000; **17**: 463–71.
14. Agardh E, Bruun A, Agardh CD. Retinal glial cell immunoreactivity and neuronal cell changes in rats with STZ-induced diabetes. *Curr Eye Res* 2001; **23**: 276–84.
15. Barber AJ, Antonetti DA, Gardner TW. Altered expression of retinal occludin and glial fibrillary acidic protein in experimental diabetes. The Penn State Retina Research Group. *Invest Ophthalmol Vis Sci* 2000; **41**: 3561–8.
16. Barber AJ, Antonetti DA. Mapping the blood vessels with paracellular permeability in the retinas of diabetic rats. *Invest Ophthalmol Vis Sci* 2003; **44**: 5410–6.
17. Pautler EL, Ennis SR. The effect of induced diabetes on the electroretinogram components of the pigmented rat. *Invest Ophthalmol Vis Sci* 1980; **19**: 702–5.
18. Sakai H, Tani Y, Shirasawa E, Shirao Y, Kawasaki K. Development of electroretinographic alterations in streptozotocin-induced diabetes in rats. *Ophthalmic Res* 1995; **27**: 57–63.
19. Li Q, Zemel E, Miller B, Perlman I. Early retinal damage in experimental diabetes: electroretinographical and morphological observations. *Exp Eye Res* 2002; **74**: 615–25.
20. Dalke C, Löster J, Fuchs H *et al.* Electroretinography as a screening method for mutations causing retinal dysfunction in mice. *Invest Ophthalmol Vis Sci* 2004; **45**: 601–9.
21. Hood DC, Shady S, Birch DG. Understanding changes in the b-wave of the ERG caused by heterogeneous receptor damage. *Invest Ophthalmol Vis Sci* 1994; **35**: 2477–88.
22. Naka KI, Rushton WA. S-potentials from luminosity units in the retina of fish (Cyprinidae). *J Physiol* 1966; **185**: 587–99.
23. Roecker EB, Pulos E, Bresnick GH, Severns M. Characterization of the electroretinographic scotopic B-wave amplitude in diabetic and normal subjects. *Invest Ophthalmol Vis Sci* 1992; **33**: 1575–83.
24. Velten IM, Horn FK, Korth M, Velten K. The b-wave of the dark adapted flash electroretinogram in patients with advanced asymmetrical glaucoma and normal subjects. *Br J Ophthalmol* 2001; **85**: 403–9.
25. Hood DC, Birch DG. Rod phototransduction in retinitis pigmentosa: estimation and interpretation of parameters derived from the rod a-wave. *Invest Ophthalmol Vis Sci* 1994; **35**: 2948–61.
26. Hood DC, Birch DG. Assessing abnormal rod photoreceptor activity with the a-wave of the electroretinogram: applications and methods. *Doc Ophthalmol* 1996; **92**: 253–67.
27. Bresnick GH. Diabetic retinopathy viewed as a neurosensory disorder. *Arch Ophthalmol* 1986; **104**: 989–90.
28. Dosso AA, Bonvin FR, Morel Y, Golay A, Assal JP, Leuenberger PM. Risk factors associated with contrast sensitivity loss in diabetic patients. *Graefes Arch Clin Exp Ophthalmol* 1996; **234**: 300–5.
29. Di Leo MA, Caputo S, Falsini B *et al.* Nonselective loss of contrast sensitivity in visual system testing in early type I diabetes. *Diabetes Care* 1992; **15**: 620–5.
30. Harris A, Arend O, Danis RP, Evans D, Wolf S, Martin BJ. Hyperoxia improves contrast sensitivity in early diabetic retinopathy. *Br J Ophthalmol* 1996; **80**: 209–13.
31. Hardy KJ, Lipton J, Scase MO, Foster DH, Scarpello JH. Detection of colour vision abnormalities in uncomplicated type 1 diabetic patients with angiographically normal retinas. *Br J Ophthalmol* 1992; **76**: 461–4.
32. Hardy KJ, Scarpello JH, Foster DH, Moreland JD. Effect of diabetes associated increases in lens optical density on colour discrimination in insulin dependent diabetes. *Br J Ophthalmol* 1994; **78**: 754–6.
33. Bresnick GH, Palta M. Oscillatory potential amplitudes. Relation to severity of diabetic retinopathy. *Arch Ophthalmol* 1987; **105**: 929–33.
34. Arden GB, Hamilton AM, Wilson-Holt J, Ryan S, Yudkin JS, Kurtz A. Pattern electroretinograms become abnormal when background diabetic retinopathy deteriorates to a preproliferative stage: possible use as a screening test. *Br J Ophthalmol* 1986; **70**: 330–5.
35. Karadeniz S, Kir N, Yilmaz MT *et al.* Alteration of visual function in impaired glucose tolerance. *Eur J Ophthalmol* 1996; **6**: 59–62.
36. Ogden TE. The oscillatory waves of the primate electroretinogram. *Vision Res* 1973; **13**: 1059–74.
37. Speros P, Price J. Oscillatory potentials. History, techniques and potential use in the evaluation of disturbances of retinal circulation. *Surv Ophthalmol* 1981; **25**: 237–52.
38. Wachtmeister L. Basic research and clinical aspects of the oscillatory potentials of the electroretinogram. *Doc Ophthalmol* 1987; **66**: 187–94.
39. Park SH, Park JW, Park SJ *et al.* Apoptotic death of photoreceptors in the streptozotocin-induced diabetic rat retina. *Diabetologia* 2003; **46**: 1260–8.

40. Do carmo A, Ramos P, Reis A, Proenca R, Cunha-vaz JG. Breakdown of the inner and outer blood retinal barrier in streptozotocin-induced diabetes. *Exp Eye Res* 1998; **67**: 569–75.
41. King-Smith PE, Loffing DH, Jones R. Rod and cone ERGs and their oscillatory potentials. *Invest Ophthalmol Vis Sci* 1986; **27**: 270–3.
42. Janaky M, Goupland SG, Benedek G. Human oscillatory potentials: components of rod origin. *Ophthalmologica* 1996; **210**: 315–8
43. Rousseau S, Lachapelle P. The electroretinogram recorded at the onset of dark-adaptation: understanding the origin of the scotopic oscillatory potentials. *Doc Ophthalmol* 1999; **99**: 135–50.
44. Goto Y, Peachey NS, Ripps H, Naash MI. Functional abnormalities in transgenic mice expressing a mutant rhodopsin gene. *Invest Ophthalmol Vis Sci* 1995; **36**: 62–71.
45. Sieving PA, Murayama K, Naarendorp F. Push-pull model of the primate photopic electroretinogram: a role for hyperpolarizing neurons in shaping the b-wave. *Vis Neurosci* 1994; **11**: 519–32.

Int Ophthalmol
DOI 10.1007/s10792-007-9150-x

PHOTOGRAPHIC ESSAY

Severe acute ocular ischemia associated with spontaneous internal carotid artery dissection

Yasuhiro Takaki · Mayuko Nagata · Kei Shinoda · Shinya Tatewaki · Kisaburo Yamada · Celso Soiti Matsumoto · Tomonobu Hazuku · Hiroyuki Yamashita · Toru Ikebe · Kazuo Nakatsuka

Received: 27 June 2007 / Accepted: 25 September 2007 ·

Abstract A healthy 40-year-old man developed unilateral ocular ischemic syndrome as the only manifestation of a spontaneous internal carotid artery dissection.

Keywords Ocular ischemic syndrome · Central retinal artery occlusion · Ophthalmic artery occlusion · Internal carotid artery dissection

Case report

A healthy 40-year-old man complained of a sudden decrease of vision in his right eye. His visual acuity was light perception OD and 1.2 OS. Ophthalmoscopy revealed a swelling of the optic disc and severe retinal edema in the posterior and peripheral retina (Fig. 1). Fluorescein angiography (FA) showed a marked delay in the arm-to-retina time and a delay in the choroidal flush (Fig. 1). Indocyanine angiography (IA) showed patchy hypofluorescent areas corresponding to the filling defects observed by FA. The *a*- and *b*-waves of the electroretinograms were decreased in the right eye, suggesting that the outer retina was also affected (Fig. 1).

A complete obstruction of right internal carotid artery (ICA) was observed by cervical magnetic resonance angiography (Fig. 2), and cerebral angiography revealed a complete obstruction and swelling at the beginning of the right ICA. However, the right cerebral artery was filled through shunt vessels from the left ICA. A diagnosis of a spontaneous ICA dissection was made, but intensive treatment including intravenous injection of urokinase, anterior chamber paracentesis, and oral acetazolamide and nitroglycerin failed to improve the vision.

Y. Takaki · M. Nagata · K. Shinoda (✉) · S. Tatewaki · K. Yamada · C. S. Matsumoto · K. Nakatsuka
Department of Brain and Neuroscience, Division of Sensory and Locomotive Science, Ophthalmology, Oita University Faculty of Medicine, Hasama-machi, Yufu-shi, Oita 879-5593, Japan
e-mail: shinodak@med.oita-u.ac.jp

T. Hazuku · H. Yamashita · T. Ikebe
Department of Ophthalmology, Oita Prefectural Hospital, Oita, Japan

Comments

Biousse et al. [1] reported that about one-third of patients with a spontaneous dissection of the ICA had a stroke within the first 2 weeks, and this was followed by ocular symptoms. Thus, a rapid evaluation of the cerebral circulation ipsilateral to an ICA dissection and proper treatment are highly important.

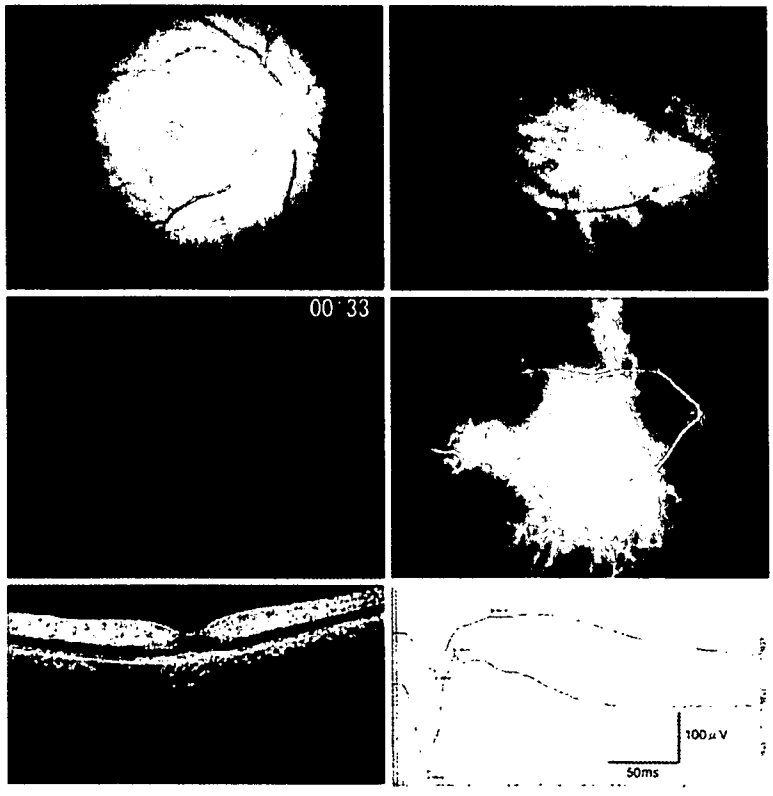

Fig. 1 Ocular findings in the right eye of a patient with a dissection of the right internal carotid artery. *Top left* Fundus photograph showing swelling of optic disc and diffuse retinal edema with a cherry-red spot. *Top right* An irregular retinal whitening of the peripheral retina is observed. *Middle left* Fluorescein fundus angiogram in the early phase showing a filling delay in retinal as well as choroidal circulations. A patchy defect of the choroidal filling is also seen. *Middle right* Indocyanine green fundus angiogram in the early phase (40 s after dye injection) showing filling defect as a patchy pattern. *Bottom left* Optical coherence tomography showing diffuse retinal thickening and disappearance of the inner segment/outer segment line. *Bottom right* Single-flash electroretinograms showing reduced amplitude and delayed implicit time of *a*- and *b*-waves in the right eye

Although various ocular symptoms were reported following a dissection of the ICA, a complete occlusion of the retinal artery or ophthalmic artery are rare [2–4] because of collateral vessels and retrograde blood flow [1]. Generally, ophthalmic symptoms usually occur in combination with other systemic signs, e.g., pulsatile tinnitus, cranial nerve palsy, head, facial, and neck pain. Thus, these changes indicate that the ocular symptoms should not be overlooked as a first indication of an ICA dissection [1, 5, 6].

In our case, an acute painless ophthalmic artery occlusion was the only clinical manifestation. We emphasize that ophthalmologist should be aware that a spontaneous ICA dissection may be the cause of ocular ischemic syndrome even in a young, otherwise healthy individuals.

Acknowledgements Support of this study was provided by Researches on Sensory and Communicative Disorders from the Ministry of Health, Labor, and Welfare, Japan. No author has a proprietary interest in any material or method mentioned.

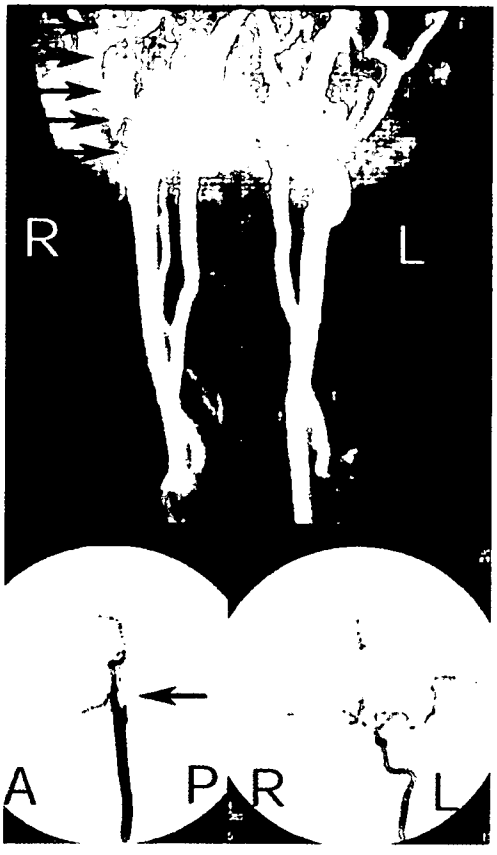

Fig. 2 Magnetic resonance angiography (MRA) of the cervix and brain, and cerebral angiography in the patient. *Top* MRA showing complete occlusion of the right internal carotid artery (ICA) indicated by *arrows*: *R* right, *L* left. *Bottom* The lateral view of the cerebral angiogram showing complete obstruction and swelling at the beginning of right ICA indicated by *arrow* (*left*). Front view of the left ICA angiogram showing intact filling of the right cerebral artery through collateral vessels from the left ICA (*right*): *A* anterior, *P* posterior, *R* right, *L* left

References

1. Biousse V, Touboul PJ, D'Anglejan-Chatillon J, Levy C, Schaison M, Bousser MG (1998) Ophthalmologic manifestations of internal carotid artery dissection. Am J Ophthalmol 126:565–577
2. McDonough RL, Forteza AM, Flynn HW Jr (1998) Internal carotid artery dissection causing a branch retinal artery occlusion in a young adult. Am J Ophthalmol 125:706–708
3. Mokhtari F, Massin P, Paques M, Biousse V, Houdart E, Blain P, Gaudric A (2000) Central retinal artery occlusion associated with head or neck pain revealing spontaneous internal carotid artery dissection. Am J Ophthalmol 129:108–109
4. Schneider U, Hermann A, Ernemann U, Bartz-Schmidt KU (2004) Central retinal artery occlusion secondary to spontaneous internal carotid artery dissection. Retina 24:979–981
5. Kerty E (1999) The ophthalmology of internal carotid artery dissection. Acta Ophthalmol Scand 77:418–421
6. Giroud M, Fayolle H, Andre N, Dumas R, Becker F, Martin D, Baudoin N, Krause D (1994) Incidence of internal carotid artery dissection in the community of Dijon. J Neurol Neurosurg Psychiatry 57:1443

Graefe's Arch Clin Exp Ophthalmol
(2007) 245: 305–308

CASE REPORT

DOI 10.1007/s00417-005-0236-8

Takefumi Yamaguchi
Makoto Inoue
Susumu Ishida
Kei Shinoda

Detecting vitreomacular adhesions in eyes with asteroid hyalosis with triamcinolone acetonide

Received: 12 September 2005
Revised: 23 October 2005
Accepted: 4 December 2005
Published online: 13 January 2006

T. Yamaguchi · M. Inoue (✉) ·
S. Ishida · K. Shinoda
Department of Ophthalmology,
Keio University, School of Medicine,
35 Shinanomachi, Shinjuku-ku,
Tokyo, 160-8582, Japan
e-mail: inoshin@sc.itc.keio.ac.jp
Tel.: +81-33353-1211
Fax: +81-33359-8302

Abstract *Background:* To report the incidence of posterior vitreous detachments (PVDs) and the surgical results of vitrectomy with intravitreal triamcinolone acetonide (TA) to detect vitreomacular adhesions in eyes with asteroid hyalosis (AH). *Methods:* Ten eyes of nine patients with AH underwent vitrectomy, six eyes with TA and four without TA. The presence of a PVD was determined preoperatively by ultrasound echography (USE) and intraoperatively by microscopic observations. The postoperative best-corrected visual acuities (BCVA) were evaluated. *Results:* The BCVA was improved by >2 Snellen lines in nine eyes and maintained at 20/20 with symptomatic improvements in the other eye. A vitreomacular adhesion was clearly seen during TA-assisted vitrectomy, and none was seen when TA was not used, even though preoperative USE showed an incomplete PVD in all eyes. The BCVA was not significantly better in eyes with TA-assisted vitrectomy than without TA-assisted vitrectomy. In one eye with vitrectomy without TA, a second surgery was required for a persistent cystoid macular edema and an epiretinal membrane. The BCVA and the edema in this eye improved after removing the epiretinal membrane. *Conclusions:* All (ten) of the eyes with AH were found to have a vitreomacular adhesion by preoperative USE and intraoperative microscopic observations. The residual vitreous over the macula is more easily detected and removed after intravitreally injected TA, but the visual acuities were not significantly different from eyes without TA.

Keywords Asteroid hyalosis · Triamcinolone acetonide · Vitreous · Vitrectomy · Vitreomacular traction

Introduction

Asteroid hyalosis (AH) is a relatively common vitreous disease in elderly patients and is characterized by deposits of glistening, lipid-containing calcium bodies in the vitreous [4]. A precise assessment of the retina may be difficult because the asteroid bodies can hamper a clear view of the posterior segment. AH does not cause significant visual impairment in most cases, but vitrectomy is beneficial when other ocular pathologic conditions are present [2, 5].

An intravitreal application of triamcinolone acetonide (TA) during vitrectomy, termed TA-assisted vitrectomy, makes the transparent vitreous gel more visible, which is helpful in the complete removal of the vitreous [6]. The purpose of this study was to determine the incidence of posterior vitreous detachments (PVDs), and the efficacy of TA-assisted vitrectomy to detect vitreomacular adhesions in eyes with AH.

Materials and methods

Ten eyes of nine patients (seven men and two women) with AH that led to visual disturbances or metamorphopsia underwent vitreous surgery by one of the authors (M.I.). Their

ages ranged from 48 to 79 years (mean 65.0±11.3 years), and the follow-up period ranged from 6 to 48 months (26.1± 12.7 months). Five eyes with mild lens opacities preoperatively had the lens extracted during the vitreous surgery to avoid a second surgery because of visual deterioration through progression of the nuclear cataract. Three eyes were pseudophakic, and the other two eyes were phakic with minimal lens opacity preoperatively.

All patients were fully informed about the purpose and possible complications of the treatment, and signed an informed consent. The Ethics Committee of Keio University approved the use of TA based on recommendation of the Institutional Review Board. The procedures used conformed to the tenets of the Declaration of Helsinki.

TA-assisted vitrectomy was performed to determine if residual vitreous cortex was present at the macula in six eyes. These were consecutive eyes and not randomly selected. Approximately 0.25 ml (10 mg) of TA (Kenacort-A, 40 mg/ml; Bristol Myers KK, Tokyo, Japan) was aspirated into a 1 ml syringe. The syringe was placed on a counter for several minutes, and the supernatant was removed after the crystals of TA had settled on the bottom to reduce the volume to 0.1 ml. Then BSS was added to make the volume up to 1 ml in the syringe. shaken to mix the TA crystals just before the intravitreal injection. Approximate 0.1 ml of this solution of TA was injected after core vitrectomy, and the TA crystals were aspirated immediately.

The TA crystals made the residual vitreous visible, which greatly aided in its complete removal. In the other four eyes, conventional vitrectomy was performed, and the residual vitreous cortex was carefully aspirated around the area of the macula.

The presence of a PVD was determined by preoperative ultrasound echography (USE, UD-1000; TOMEI Co, Nagoya, Japan) with or without eye movements, and also confirmed intraoperatively under the surgical microscope.

The postoperative best-corrected visual acuity (BCVA) of the six eyes with TA-assisted vitrectomy was compared with that of the four eyes with vitrectomy without TA. Statistical analysis was performed by unpaired *t*-tests.

Results

High echographic signals from the vitreous indicated the presence of the asteroid bodies, but the high signals were reduced in the premacular space (Fig. 1). This low-signal space was interpreted as being due to a PVD when USE was done without eye movement (static USE). However, a vitreoretinal adhesion with an incomplete PVD was detected in all eyes by observing less movement of the vitreous gel at the macula during USE with eye movements (dynamic USE, Table 1). In one eye, the posterior vitreous was also attached at the optic disc.

Preoperative fluorescein angiography showed macular edema in two eyes (cases 2 and 9). Intraoperative microscopic observations showed an elevation of the fovea in three eyes indicating macular edema, and parafoveal cysts in two eyes indicating cystoid macular edema (CME). The macular edema resolved postoperatively in all eyes.

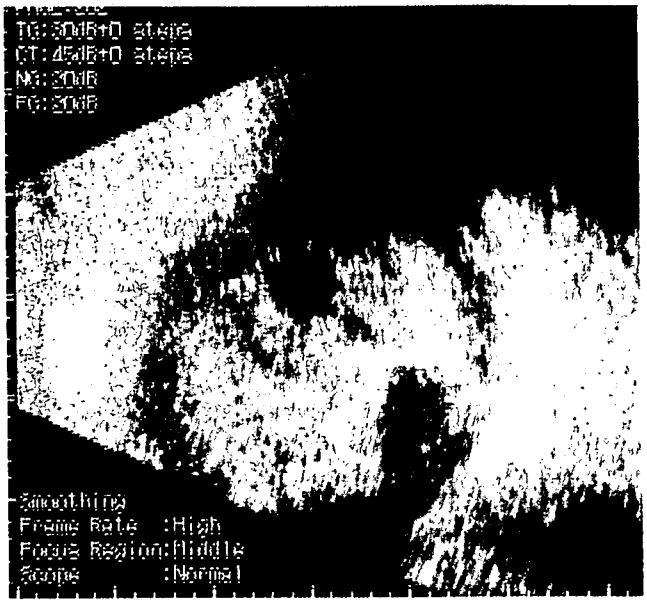

Fig. 1 Ultrasound echogram of case 1. Echogram showing high signals from the vitreous body indicating intravitreal asteroid bodies. Interestingly, the signals are reduced in the area of the vitreomacular attachment (*arrow*) showing low-echo space, suggesting an incomplete posterior vitreous detachment

Preoperatively, a focal adhesion of residual vitreous was observed at the macula in five eyes, and a diffuse vitreous adhesion in one eye, in the six eyes with TA-assisted vitrectomy. An improvement of two or more Snellen lines in the BCVA was achieved in nine eyes, and the mean improvement was 3.5 lines. In the remaining eye, there was an improvement of metamorphopsia while maintaining 20/20 vision. The mean visual improvement was 3.8 lines in eyes with TA-assisted vitrectomy, and 3.0 lines without TA-assisted vitrectomy. This difference in improvement was not significant (P=0.61, unpaired *t*-test).

The transparent vitreous at the macula was made more visible by the white TA crystals in the six eyes with TA-assisted vitrectomy (Fig. 2). The area of transparent vitreous remaining at the macula corresponded with the low-signal space in the preoperative USE.

As postoperative complications, one eye (case 2) required a cataract extraction for a cataract that developed postoperatively resulting in a visual deterioration to 20/50 from 20/30. The BCVA improved to 20/25 without any recurrent macular edema. Another eye (case 9) had an initial vitrectomy without TA because of macular edema associated with AH. Vision improved to 20/25 from 20/50, but this eye required a second vitrectomy for recurrent persistent CME and an epiretinal membrane resulting in a visual acuity of 20/30. The vision improved to 20/20 after

Table 1 Profile of patients with asteroid hyalosis

Case	Age (years)	Gender	Symptom	VM adhesion	Visual acuity		Surgery	TA-assisted vitrectomy	Pre-op and intra-op condition	Follow-up (months)	Post-op condition
					Pre-op	Post-op					
1 OD	69	W	VA, Met	+	20/100	20/25	PPV, PEA, IOL	+(spot)	Macular edema	30	
1 OS			VA, Met	+	20/60	20/25	PPV, PEA, IOL	+(spot)	Macular edema	30	
2	48	M	VA, Met	+	20/60	20/25	PPV	+(spot)	Macular edema	48	*Cataract
3	79	M	VA	+	20/20	20/20	PPV	+(spot)	Glaucoma	16	
4	63	M	VA	+	20/25	20/18	PPV	+(spot)		6	
5	79	M	VA	+	20/50	20/25	PPV, PEA, IOL	+(diffuse)		8	
6	70	F	VA	+	20/40	20/20	PPV, PEA, IOL	-	CME	32	
7	70	M	VA	+	20/25	20/18	PPV, PEA, IOL	-		30	
8	54	M	VA	+	20/25	20/20	PPV	-		27	
9	53	M	VA, Met	+	20/50	20/20	PPV	-	CME	34	*Cataract, *ERM

M male, *F* female, *VA* symptomatically decreased visual acuity, *Met* symptomatic metamorphopasia, *VM adhesion* vitreomacular adhesion by echogram. *pre-op* preoperative, *post-op* postoperative, *PPV* pars plana vitrectomy, *PEA* phacoemulsification and aspiration, *IOL* insertion of intraocular lens, *TA* triamcinolone acetonide, *+(spot)* residual vitreous visualized as white spot above the macula or diffuse sheet; +(diffuse), *CME* cystoid macular edema, **cataract* cataract developed postoperatively and surgery was performed, **ERM* postoperatively developed epiretinal membrane was removed at the second surgery

the epiretinal membrane was removed and the cataract was extracted during the second vitrectomy. None of the eyes with TA-assisted vitrectomy developed an epiretinal membrane or macular edema postoperatively.

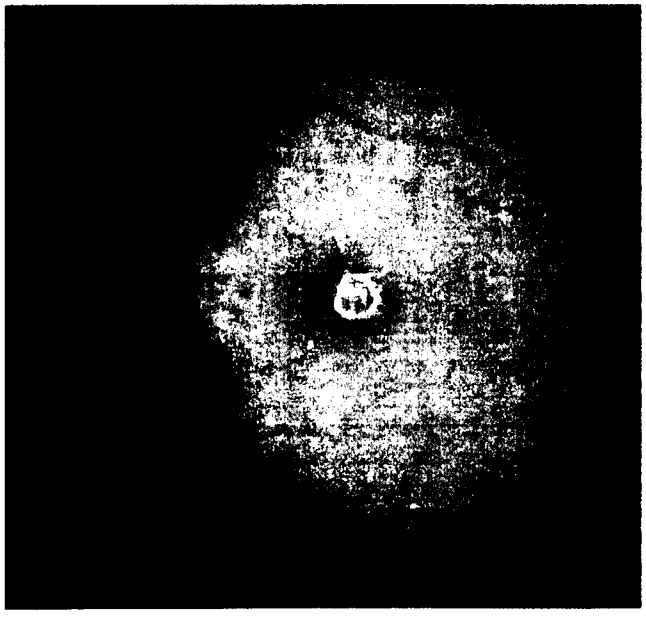

Fig. 2 Intraoperatively microscopic photograph of case 1. Photograph from intraoperative video recording showing vitreomacular adhesion of residual vitreous cortex which was made visible by intravitreally injected triamcinolone acetonide

Discussion

How AH leads to visual symptoms is not completely known. In addition, the indications for vitrectomy in patients with AH have not been definitively determined. Previous studies suggested that vitrectomy was beneficial only in selected patients who required laser photocoagulation, or those who had an unexplained visual loss and a good view of the fundus could not be made. [2] Parnes et al. reported that nine of ten eyes with AH had an improvement of vision of at least one line after vitrectomy, but they did not use TA if macular disease did not exist. [5] These results suggest that vitrectomy alone can improve the visual acuity by simply removing the vitreal opacities.

A PVD is relatively rare in patients with AH and diabetic retinopathy, [8] and a strong adhesion between the retina and vitreous is reported to be present in patients who had undergone vitrectomy for diseases associated with AH and proliferative diabetic retinopathy. [3] This was confirmed in our study, as all of our cases demonstrated a vitreous adhesion at the macula intraoperatively. These findings indicate that AH might increase the degree of vitreomacular adhesion. Interestingly, we did not extract any publications that reported a high incidence of vitreomacular adhesion

detected by ophthalmoscopy or USE in eyes with AH, but without diabetic retinopathy.

Although the number of patients studied was small, residual vitreous cortex was detected by TA-assisted vitrectomy in all of the six eyes with AH, which is higher than that in other retinal diseases undergoing TA-assisted vitrectomy, e.g. 90% in proliferative diabetic retinopathy, 77% in diabetic macular edema, 41% in branch vein retinal occlusion, and 60% in rhegmatogenous retinal detachment [7].

Browning et al. [1] reported a vitreomacular adhesion detected by an optical coherence tomography (OCT) in a patient with diabetic macular edema and AH as was also reported earlier. [3] However, there were no diabetic patients in our series, and a clear OCT image was not obtained from the six eyes with AH that had preoperative OCT. The absence of the high echographic signals from the asteroid bodies in the area of the vitreomacular attachment made it difficult to detect vitreomacular adhesion in static echograms. This absence of signals might be a limitation of USE, but the ophthalmoscopic observations suggested that the vitreous attached to the macula had fewer asteroid bodies than the central vitreous. Thus, conventional vitrectomy may fail to remove vitreomacular adhesions completely because the residual vitreous is less visible with fewer asteroid bodies.

A high incidence of vitreomacular adhesions was found in eyes with AH by preoperative USE and intraoperative observations. Residual vitreous cortex can lead to the formation of epiretinal membranes that cause persistent tangential macular traction, and a complete removal of vitreomacular traction by TA-assisted vitrectomy may provide better visual outcome in vitrectomy in eyes with AH. However, residual vitreous over the macula is better seen and removed with TA, but the visual acuity did not seem to be better with the TA in this small series. In addition, simultaneous cataract surgery for minimal lens opacities may have affected the visual outcomes in the half of the cases. Further studies with functional and morphologic analysis are needed.

Acknowledgement None of the authors has a financial or proprietary interest in any material or methods mentioned.

References

1. Browning DJ, Fraser CM (2004) Optical coherence tomography to detect macular edema in the presence of asteroid hyalosis. Am J Ophthalmol 137:959–961
2. Feist RM, Morris RE, Witherspoon CD et al (1990) Virectomy in asteroid hyalosis. Retina 10:173–177
3. Ikeda T, Sawa H, Koizumi K et al (1998) Vitrectomy for proliferative diabetic retinopathy with asteroid hyalosis. Retina 18:410–414
4. Moss SE, Klein R, Klein BEK (2001) Asteroid hyalosis in a population: the beaver dam eye study. Am J Ophthalmol 132:70–75
5. Parnes RE, Zakov ZN, Novak MA, Rice TA (1998) Virectomy in patients with decreased visual acuity secondary to asteroid hyalosis. Am J Ophthalmol 125:703–704
6. Peyman GA, Cheema R, Conway MD, Fang T (2000) Triamcinolone acetonide as an aid to visualization of the vitreous and the posterior hyaloid during pars plana vitrectomy. Retina 20:554–555
7. Sonoda K, Sakamoto T, Enaida H et al (2004) Residual vitreous cortex after surgical posterior vitreous separation visualized by intravitreous triamcinolone acetonide. Ophthalmology 111:226–230
8. Wasano T, Hirokawa H, Tagawa H et al (1987) Asteroid hyalosis: posterior vitreous detachment and diabetic retinopathy. Ann Ophthalmol 19:255–258

Current Eye Research, 32:773–779, 2007

ISSN: 0271-3683 print / 1460-2202 online
DOI: 10.1080/02713680701531108

informa
healthcare

Microcirculation in Eyes After Rhegmatogenous Retinal Detachment Surgery

Enrique Adan Sato
Department of Ophthalmology, Keio University School of Medicine, Tokyo, Japan

Kei Shinoda
Department of Ophthalmology, Keio University School of Medicine, Tokyo, Japan; and Laboratory of Visual Physiology, National Institute of Sensory Organs, Tokyo, Japan

Itaru Kimura, Yuichiro Ohtake, and Makoto Inoue
Department of Ophthalmology, Keio University School of Medicine, Tokyo, Japan

ABSTRACT *Purpose*: To investigate the tissue blood flow in the neuroretinal rim of the optic disk and macula after rhegmatogenous retinal detachment (RRD) surgery. *Methods*: Tissue blood flow in the neuroretinal rim of the optic disk and macula was measured with the Heidelberg retina flowmeter in 53 eyes of 53 patients who had undergone successful surgery for unilateral RRD. Patients were divided into three groups; those who had the RRD treated by conventional encircling scleral buckling (group E), by local buckling (group L), and by primary vitrectomy (group V). Blood flow measurements were made more than 6 months after surgery in a 10° × 2.5° area of the superior and inferior margins of the neuroretinal disk rim and of the superior and inferior macula area. The mean blood flow (MBF) and the ratio of the MBF in the affected eye to the healthy fellow eye (*a/f* ratio) were compared among the three groups. The influence of several clinical factors on the MBF was also investigated. *Results*: The MBF rate and mean *a/f* ratios of the MBF of the three groups were not significantly different. Multiple regression analysis revealed that the averaged MBF both at superior and inferior disk rims was significantly correlated with only the gas tamponade procedure. *Conclusions*: The ocular microcirculation is normal 6 months after scleral buckling or vitrectomy for RRD. However, the use of gas tamponade might have a subclinical adverse effect on the circulation in the neuroretinal disk rim.

KEYWORDS gas tamponade; rhegmatogenous retinal detachment; scleral buckling; tissue blood flow; vitrectomy

INTRODUCTION

The adverse effect of scleral buckling on ocular circulation has been reported from the results of experimental and clinical studies.[1–6] We have reported that the disturbances of retinal microcirculation in the macular area was correlated with the extent of rhegmatogenous retinal detachment (RRD) and was present in patients even without macular involvement. The decrease in circulation recovered to normal within 1 month after the buckling surgery.[6]

However, several cases have been reported on progressive visual field defects (VFDs) after retinal reattachment surgery using encircling buckling for

Received 19 October 2005
Accepted 20 June 2007

Correspondence: Itaru Kimura, M.D., Department of Ophthalmology, Keio University School of Medicine, 35 Shinanomachi, Shinjuku-ku, Tokyo 160-8582, Japan. E-mail: kimura@sc.itc.keio.ac.jp

peripheral RRD.[7] In these cases, the ocular blood flow, especially the tissue blood flow in the neuroretinal rim of the optic disk, was significantly lower than that of the unaffected fellow eye. Interestingly, the blood flow improved after loosening or removing the encircling buckle, suggesting that the decreased blood flow was caused by the encircling buckle even after successful reattachment of the retina.

These findings prompted us to investigate the tissue blood flow in the macular area and the neuroretinal rim of the optic disk in patients who had successful RRD surgery. The results obtained from patients who had either primary vitrectomy or scleral buckling with local or encircling buckle were compared. We also investigated the clinical factors including the surgical procedures and fundus findings that might be related to ocular microcirculation in eyes more than 6 months after successful retinal detachment surgery.

MATERIALS AND METHODS

Subjects

There were 53 patients (29 men and 24 women) with RRD whose ages ranged from 12 to 78 years with a mean of 48.8 ± 14.6 (standard deviation) years. The procedures used conformed to the tenets of the Declaration of Helsinki, and an informed consent was obtained from all patients before the measurements.

In all patients, the RRD was successfully reattached by either scleral buckling or vitrectomy under local anesthesia. The patients were divided into three groups according to the surgical procedures: group E had encircling scleral buckling, group L had local buckling, and group V had primary vitrectomy.

The scleral buckling procedures included transscleral cryotherapy, transscleral drainage of subretinal fluid in 14 of 23 in group E and 11 of 19 patients in group L, and intravitreal gas tamponade in 11 and 7 patients in groups E and L, respectively. In groups E and L, the buckling materials were placed as exoplants. In 14 eyes in group E, a silicone band (no. 240, MIRA) in combination with a silicone tire (no. 220, 277, 276, or 287, MIRA) and a silicone sleeve (no. 270, MIRA) were used, and in 9 eyes, a silicone sponge (no. 506 or 501, MIRA) was used. In group L, a silicone sponge (no. 506 or 501, MIRA) was placed circumferentially as an exoplant.

For primary vitrectomy, the core vitreous was removed, and the peripheral vitreous gel including that around the retinal break was shaved off. Then, the subretinal fluid was drained through the original retinal break in 10 eyes or through an intentional retinal break in 1 eye during fluid/air exchange and intravitreal gas injection. Cataract surgery was combined with the RRD surgery in four eyes. Silicone oil was not used for tamponade in any of the eyes. Intraoperative complications were not encountered, and a reattachment of the retina was achieved in all patients by the initial surgery.

Only patients with a best corrected visual acuity ≥20/20 in both affected and fellow eyes were studied. The exclusion criteria were ophthalmic diseases such as uveitis, glaucoma, cataract that affected visual acuity, and use of any medication (e.g., corticosteroids, β-blockers, calcium channel blockers, angiotensin-converting enzyme inhibitors, platelet active agents, and carbonic anhydrase inhibitors) except postoperative antibiotics and anti-inflammatory agents during the 2 weeks before the measurements. In addition, patients with systemic hypertension, cardiovascular diseases, endocrine disease, and an intraocular pressure (IOP) not within the range 10–19 mmHg were excluded.

Blood Flow Measurements

The tissue blood flow was measured more than 6 months after the surgery with a range from 6 to 78 months (18.9 ± 16.9 months; Tables 1 and 2). After the measurement of the IOP by applanation tonometry, the tissue blood flow was measured in both eyes by scanning laser Doppler flowmetry (SLDF) using the Heidelberg retina flowmeter (HRF, Heidelberg Engineering, Heidelberg, Germany). The principle, validity, and reliability of SLDF in measuring ocular blood flow have been established.[8,9]

The areas measured were the superior and inferior area of the macula and the superior and inferior neuroretinal rim area. The measurements were repeated at least three times in a 10° × 2.5° area (Fig. 1). Each area was divided into 64 lines with 256 points/line, and each line was scanned 128 times. The measurement was simultaneously performed in the area between the

TABLE 1 Patients demographics

	Group E	Group L	Group V
Number	23	19	11
Gender (male:female)	13:10	9:10	7:4
Age (years old, mean ± S.D.)	43.8 ± 15.0	49.9 ± 14.8	57.5 ± 8.4

TABLE 2 Summarized clinical findings of the operated eye

	Group E	Group L	Group V
Extent of retinal detachment (hr)	3.9 ± 1.6	3.4 ± 1.4	4.9 ± 1.6
Macular involvement number (%)	8 (34.8)	2 (10.5)	3 (37.5)
Transscleral SFR drainage number (%)	14 (60.9)	11 (57.9)	0 (0)
Gas tamponade number (%)	11 (47.8)	7 (36.8)	11 (100)
Period after surgery (months, mean ± SD)	19.6 ± 19.8	16.7 ± 12.0	21.5 ± 18.4
logMAR (mean ± SD)			
Before surgery	0.18 ± 0.51	0.03 ± 0.18	0.37 ± 0.73
At MBF measurement	−0.04 ± 0.04	−0.04 ± 0.04	−0.04 ± 0.04
Refractive error at MBF measurement (diopter, mean ± SD)	−3.6 ± 3.9	−2.9 ± 2.8	−3.3 ± 3.2
IOP at MBF measurement (mmHg, mean ± SD)	13.2 ± 2.8	15.0 ± 2.8	14.2 ± 1.5

SRF, subretinal fluid; MAR, minimal angle resolution; MBF, mean blood flow; IOP, intraocular pressure.

concentric semicircular lines along the neuroretinal rim (Fig. 1).

The mean blood flow (MBF) was calculated as an indicator of tissue microcirculation by the automatic full-field perfusion image analyzer.[10] Ophthalmoscopically visible vessels were automatically excluded from the measurements, and the MBF values are given in arbitrary units (AU). The MBF ratio, affected eye/fellow eye (*a/f*), was calculated to minimize the interexaminations variations. It has been shown that the *a/f* ratio is a good measure of the changes in retinal circulation because the MBF between the two eyes of normal subjects are not significantly different.[11]

All measurements were performed without pupillary dilation, and patients were asked to fixate a distant target during the measurements. A moveable fixation point was used to allow the positioning of the examined eye. Several images were then acquired in the superior and the inferior areas. Great care was taken to measure the same retinal areas repeatedly by using visible vessels and the optic disk margin as landmarks on the video monitor.

Three selected SLDF images were analyzed in each eye, and the average of the measurements from the three images was used for analysis. All images were analyzed by the same masked observer. The averaged MBF or the *a/f* ratio of the MBF was used for statistical evaluation. Poor-quality images, mainly due to large eye movements and poor fixation, were excluded from the analysis.

Indirect ophthalmoscopy and slit-lamp biomicroscopy with a +90 diopter lens showed that all of the eyes were normal, and no abnormalities were detected within the vascular arcade including the macula.

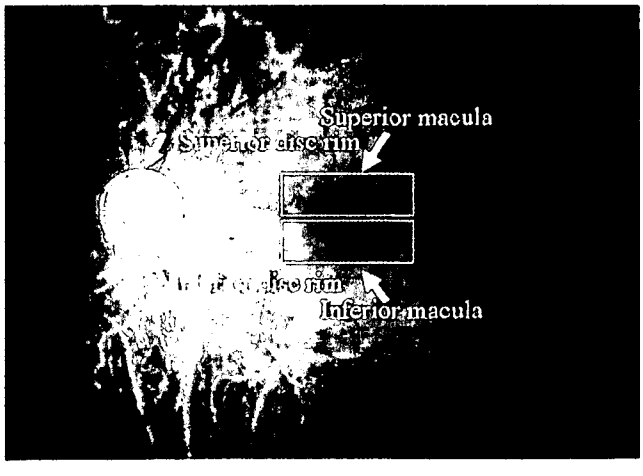

FIGURE 1 Measurement regions at the neuroretinal disk rim and macular area. Each area was divided into superior and inferior areas. Each measurement was performed three or more times and analyzed by scanning laser Doppler flowmetry.

Statistical Analysis

The results are presented as mean ± standard deviation (SD) unless otherwise indicated. The age, gender, IOP, averaged MBF, and *a/f* ratios of the MBF were compared among the three groups using Kruskal-Walllis test. Clinical factors such as age, gender, preoperative visual acuity (logMAR units), refractive error, size of retinal detachment, presence of macular detachment, surgical procedures, use of gas tamponade, transscleral subretinal fluid drainage, time after surgery, visual acuity at time of MBF measurement, and IOP at MBF measurement associated with MBF were determined by multiple regression analysis as independent variables